Solar Phys (2015) 290:1947–1961
DOI 10.1007/s11207-015-0738-4

A Simple Way to Estimate the Soft X-ray Class of Far-Side Solar Flares Observed with STEREO/EUVI

I.M. Chertok[1] · A.V. Belov[1] · V.V. Grechnev[2]

Received: 6 May 2015 / Accepted: 4 July 2015 / Published online: 18 July 2015

Abstract Around the peaks of substantial flares, bright spurious nearly horizontal saturation streaks (B-streaks) corresponding to the brightest parts of the flare sources appear in the STEREO/EUVI 195 Å images. We show that the length of these B-streaks can be used to solve the problem of evaluating the soft X-ray flux and class of far-side flares that are registered with the twin STEREO spacecraft, but are invisible from Earth. For this purpose, from data on about 350 flares that were observed from January 2007 to July 2014 (mainly exceeding the GOES M1.0 level) both with GOES and STEREO, we established an empirical relation that correlates the GOES 1 – 8 Å peak flux and the B-streak length. This allowed us to estimate the soft X-ray classes for approximately 65 strong far-side flares observed by STEREO for the same years. The results of this simple and prompt method are consistent with the estimations of Nitta *et al.* (*Solar Phys.* **288**, 241, 2013a) that were based on the calculations of the EUVI full-disk digital number output. In addition, we studied some features of the B-streaks in impulsive and long-duration flares and demonstrate that B-streaks in several consecutive EUVI images can be used to reconstruct a probable time history of strong far-side flares.

Keywords STEREO · Extreme ultraviolet · Solar flares · Saturation streaks · GOES · Soft X-rays

✉ V.V. Grechnev
grechnev@iszf.irk.ru

I.M. Chertok
ichertok@izmiran.ru

A.V. Belov
abelov@izmiran.ru

1 Pushkov Institute of Terrestrial Magnetism, Ionosphere and Radio Wave Propagation (IZMIRAN), Troitsk, Moscow 142190, Russia

2 Institute of Solar-Terrestrial Physics SB RAS, Lermontov St. 126A, Irkutsk 664033, Russia

1. Introduction

In October 2006, the twin *Solar Terrestrial Relations Observatory* (STEREO; Kaiser *et al.*, 2008) spacecraft was launched, and at the end of January 2007, the two spacecraft separated and entered into heliocentric orbits near 1 AU in opposite directions. The *Ahead* (A) probe leads the Earth, while the *Behind* (B) probe lags behind the Earth, drifting about 22° per year from the Sun–Earth line. In February 2011, the two STEREO spacecraft were already in quadrature with the Earth, providing the first-ever complete 360° view of the Sun. At the end of July 2014, the two spacecraft were located on opposite sides of the Earth's orbit; STEREO-A was ahead of the Earth by 164°, and STEREO-B was 162° behind the Earth. The twin STEREO spacecraft are equipped with almost identical sets of extreme-ultraviolet, optical, radio, and in situ instruments. In particular, the *Sun Earth Connection Coronal and Heliospheric Investigation suit* (SECCHI; Howard *et al.*, 2008) includes the *Extreme Ultraviolet Imager* (EUVI; Wuelser *et al.*, 2004), which provides solar images in four channels at 171, 195, 284, and 304 Å.

With an increase of the longitudinal separation between the two STEREO spacecraft and each of them with the Sun–Earth line, the number of flares registered with the A and/or B probes that are invisible from Earth has been growing. Among the problems that are investigated in studies of the backside flares, one is classifying their importance, which would allow one to compare them with flares recorded by near-Earth satellites. STEREO observations and information about the importance of far-side flares are significant for investigations of solar activity phenomena such as flares themselves, eruptions, large-scale coronal waves, coronal mass ejections (CMEs), and solar energetic particles (SEPs). These observational studies are promising to achieve further progress in understanding and modeling these phenomena as well as space weather forecasting (e.g., Hudson, 2011; Lugaz *et al.*, 2012; Webb and Howard, 2012; Nitta *et al.* 2013a, 2013b; Aschwanden *et al.*, 2014; Li *et al.*, 2014; Richardson *et al.*, 2014; Kwon, Zhang, and Vourlidas, 2015). In addition to the classification of flares based on the intensity and emission area in the Hα line, the soft X-ray (SXR) flare classification is currently generally accepted and widely used. The C, M, and X SXR classes of flares are determined according to the peak fluxes measured by the *Geostationary Operational Environmental Satellite* (GOES; Garcia, 1994) 1 – 8 Å detectors in the ranges of $(1-10)\times10^{-6}$, 10^{-5}, and 10^{-4} W m^{-2}, respectively.

Nitta *et al.* (2013a) addressed the problem of classifying the STEREO backside flares by calculating the EUVI 195 Å full-disk emission fluxes as the total output of the charge-coupled device (CCD) camera in units of digital data number (DN) per second. Using data from June 2010 to September 2012, the authors selected the flares that were recorded by GOES and simultaneously were observed with one or both STEREO spacecraft. They found an empirical relation between the observed GOES 1 – 8 Å peak fluxes and the calculated EUVI 195 Å full-disk DN output. Using this relation, one can estimate the GOES peak X-ray flux of sufficiently intense backside flares that are observed only by STEREO. Nitta *et al.* (2013a) presented a list of 16 such major far-side flares detected with this procedure.

In the present paper, we propose a somewhat simpler technique for estimations of the X-ray class of STEREO flares. The technique is based on the measurements of the length of a bright spurious saturation streak, which appears in the EUVI 195 Å images nearly along its East–West axis around the peaks of sufficiently strong flares (Figure 1). This streak is a consequence of the so-called blooming, *i.e.*, saturation of CCD cells, corresponding to the brightest part of a flare source, and spilling of excessive electrons from these cells along CCD columns (see Wuelser *et al.*, 2004). Similar overexposure effects also occur in the *Extreme ultraviolet Imaging Telescope* (EIT; Delaboudinière *et al.*, 1995) images gathered

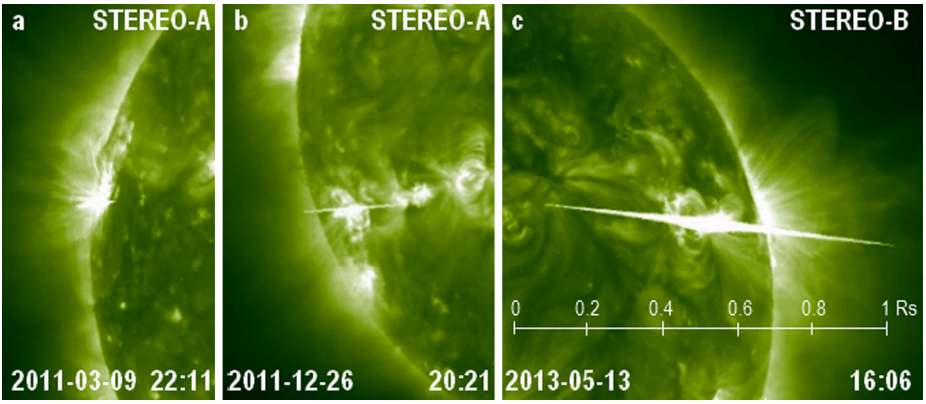

Figure 1 The STEREO/EUVI 195 Å B-streaks typical of C-, M-, and X-class flares. The spatial scale shown in panel (c) is the same for all of the three images. The 09 March 2011, 26 December 2011, and 13 May 2013 flares are labeled 77, 157, and 295 in Figure 2 (see also Table 1).

with SOHO (*e.g.*, Andrews, 2001) and in the *Atmospheric Imaging Assembly* (AIA; Lemen *et al.*, 2012) images obtained with SDO (Schwartz, Torre, and Piana, 2014).

We refer to the blooming streaks as B-streaks throughout. The B-streaks affect the images of flare cores around the peak time. These sources and moments are physically most interesting. The B-streaks are usually considered as a serious interference for the image processing and studies. Our analysis shows, however, that B-streaks contain useful information about the flare importance and the brightest EUV sources in general. This idea is based on the fact that the stronger emission flux produces stronger blooming in CCD cells, and therefore a longer B-streak is formed (see Figure 1). In Section 2, we describe our approach and data selected for the analysis. Section 3 is devoted to strong flares observed with both GOES and one or two STEREO spacecraft. These concurrent observations allowed us to obtain an empirical relation between the relative lengths of B-streaks and the SXR fluxes (*i.e.*, the GOES classes) of the STEREO flares. In Section 4, we present examples and a list of major backside flares (mainly above the M3.0 class), registered by the STEREO spacecraft in 2007 – 2014. We also compare the SXR classes of far-side flares evaluated by Nitta *et al.* (2013a), using the calculated DN fluxes in the EUVI 195 Å channel, and those estimated with our technique. We finish in Section 5 with a summary and concluding remarks.

2. Approach and Data

To determine to which extent B-streaks are suitable for an assessment of the SXR class of backside flares, it is necessary to analyze the relationship between these parameters for coincident flares that are observed simultaneously with GOES and one or both STEREO spacecraft. Proceeding from the STEREO trajectories, it is clear that the number of such coincident flares was initially large, but then gradually decreased. After February 2011, when the two STEREO spacecraft were in the near-quadrature configuration relative to the Sun–Earth line, only those flares were observed with GOES and one of the STEREO probes that were sufficiently removed from the central meridian visible from Earth. In 2013 and 2014, only near-the-limb flares, from the Earth view, could be observed with GOES and one of the STEREO spacecraft; the west- and east-limb GOES flares were observed with A and B, respectively.

We have analyzed the NOAA GOES flare list up to July 2014, *i.e.*, during the ascent and maximum phases of Solar Cycle 24, (ftp://ftp.ngdc.noaa.gov/STP/space-weather/solar-data/solar-features/solar-flares/x-rays/goes/) and selected for further analysis practically all coincident flares above the M1.0 class. The exceptions were a small number of flares overlapping in time, but occurring in different active regions; flares with obvious partial limb occultation for either STEREO or GOES; and some M1–M2 flares, in which a relatively short B-streak was not discernible against extended pre-existing structures. In addition to strong flares, a certain number of C-class flares with a visible B-streak was randomly chosen to be included in our analysis. We considered these events to reveal more clearly the tendency of the increasing length of the EUV B-streak with an increasing SXR flare importance.

For the considerations of B-streaks we used EUVI images in the 195 Å channel, which encompasses the Fe XII line with a peak temperature of ≈ 1.5 MK, because these images were produced mostly every five minutes (sometimes the cadence was 2.5 or ten minutes). More importantly, this channel has some sensitivity to the emission of high-temperature plasma due to the secondary peak around 15 MK in the Fe XXIV line at 192 Å that makes the 195 Å channel the closest analog of the SXR GOES monitors (see Nitta *et al.*, 2013a). As the main quantitative parameter characterizing B-streaks, we took its maximum length, L, measured in fractions of the solar radius, R_S, in the same EUVI image, *i.e.*, the L/R_S ratio. As we show below, the length of a B-streak can considerably exceed $1R_S$ in major flares.

We endeavored to develop a method that would be as simple as possible. For this reason, we did not analyze the source FITS files and instead used the EUVI 195 Å images in JPEG and movies in MPEG, which are available at http://stereo-ssc.nascom.nasa.gov/browse/. They are already processed with the standard SolarSoft routine secchi_prep.pro and rotated so that solar north is up. In spite of their nonlinear brightness scale, most B-streaks are clearly discernible in the 512×512 movies. We also used the 2048×2048 images to measure the B-streak length, especially for weak flares. The observed B-streak length is expected to depend on the exposure time, τ_{exp}. For each image, information on τ_{exp} can be found at http://sharpp.nrl.navy.mil/cgi-bin/swdbi/secchi_flight/img_short/form, using the full-page output. More often than not, the EUVI telescopes operated with $\tau_{exp} = 8$ s. The 16 s exposure time was almost regularly used in early observations until January 2010. Later on, $\tau_{exp} = 16$ s was only used for the images every even hour at the 16th minute, *i.e.*, at 00:16, 02:16, 04:16, and so on (*all times hereafter refer to UT*). We corrected all the considered images to $\tau_{exp} = 8$ s. To be precise, if the longest B-streak occurred in an image with $\tau_{exp} = 16$ s, we halved its length and compared it with B-streaks in adjacent images. We then excluded flares (mainly of C-class) in which after this correction the maximum relative length of B-streaks, L/R_S, was shorter than 0.1. The reason is that short B-streaks in these events might become visible against the background of other flare structures just because $\tau_{exp} = 16$ s.

The list of events selected for our analysis contains about 275 flares, whose GOES importance was M1 or higher, and 75 C-class flares. The complete list of flares observed with both GOES and STEREO/EUVI is accessible at http://www.izmiran.ru/~ichertok/STEREO/. Table 1 presents some flares extracted from this list and contains, in particular, those events that are mentioned below, as well as a number of major flares. Column 1 presents the serial number of a flare in the complete list. Columns 2 – 7 contain information on GOES SXR observations of a flare in 1 – 8 Å, including date, peak time, GOES class, corresponding SXR flux, F_G, in units of 10^{-6} W m^{-2}, coordinates, and the NOAA number of an active region. Columns 8 – 10 specify STEREO A or B spacecraft, the observation time of the B-streak (rounded to one minute), and its maximum relative length, L/R_S.

Table 1 Extract from the list of flares registered with GOES and STEREO (see Section 2).

No.	GOES SXR						STEREO		
	Date	Time UT	Class	Flux F_G	Location	AR	A/B	Time UT	L/R_S
(1)	(2)	(3)	(4)	(5)	(6)	(7)	(8)	(9)	(10)
17	2010-02-06	18:59	M2.9	29	N21 E17	11 045	A	19:03	0.34
27	2010-02-12	11:26	M8.3	83	N26 E11	11 046	B	11:26	0.54
77*	2011-03-09	22:12	C9.4	9.4	N08 W04	11 166	A	22:11	0.11
78	2011-03-09	23:23	X1.5	150	N08 W09	11 166	A	23:26	0.27
99	2011-07-30	02:09	M9.3	93	N16 E19	11 261	B	02:11	0.60
107	2011-08-09	08:05	X6.9	690	N17 W69	11 263	A	08:06	1.59
112	2011-09-06	22:18	X2.1	210	N14 W18	11 283	A	22:21	0.61
113	2011-09-07	22:38	X1.8	180	N14 W28	11 283	A	22:41	0.61
121	2011-09-22	11:01	X1.4	140	N13 E78	11 302	B	10:56	0.19
123	2011-09-24	09:40	X1.9	190	N12 E60	11 302	B	09:41	0.77
142	2011-11-03	20:27	X1.9	190	N22 E63	11 339	B	20:26	0.53
157	2011-12-26	20:30	M2.3	23	S21 W42	11 387	A	20:21	0.26
171	2012-01-27	18:37	X1.7	170	N27 W71	11 402	A	18:51	0.40
177*	2012-03-05	04:09	X1.1	110	N16 E54	11 429	B	04:16	0.25
189*	2012-03-07	00:24	X5.4	540	N17 E27	11 429	B	00:26	0.66
233	2012-07-06	23:08	X1.1	110	S18 W52	11 515	A	23:11	0.42
275	2012-10-23	03:17	X1.8	180	S13 E52	11 598	B	03:21	0.47
294*	2013-05-13	02:17	X1.7	170	N12 E78	11 748	B	02:16	0.42
295*	2013-05-13	16:01	X2.8	280	N11 E85	11 748	B	16:06	0.95
296	2013-05-14	01:11	X3.2	320	N13 E81	11 748	B	01:11	0.77
297	2013-05-15	01:48	X1.2	120	N12 E64	11 748	B	01:46	0.37
307	2013-10-25	08:01	X1.7	170	S04 E72	11 882	B	08:03	0.38
308	2013-10-25	15:03	X2.1	210	S03 E68	11 882	B	15:01	0.64
315*	2013-10-28	02:03	X1.0	100	N04 W66	11 875	A	02:06	0.24
319	2013-10-29	21:54	X2.3	230	N08 W86	11 875	A	21:56	0.58
321	2013-11-19	10:26	X1.0	100	S13 W79	11 893	A	10:26	0.38
337	2014-02-25	00:49	X4.9	490	S12 E82	11 990	B	00:51	0.56
346	2014-04-25	00:27	X1.3	130	S15 W90	12 046	A	00:26	0.59
347	2014-06-10	11:42	X2.2	220	S15 E80	12 087	B	11:41	0.27
348	2014-06-10	12:52	X1.5	150	S17 E82	12 087	B	12:56	0.23

Asterisks mark the events in which the correction for an exposure time of 8 s was applied.

3. Relation Between the GOES Flux and EUVI B-Streak

In the preceding section, we described how we corrected for the EUVI exposure time. Some other factors can affect the relations between the lengths of the EUVI B-streaks and the GOES SXR fluxes. These are

- different temperature responses of the SXR GOES detectors and the EUVI 195 Å channel, as mentioned in Section 2,
- possible time difference between the flare peak in SXR and EUV emissions,
- limited imaging rate of the EUVI (Section 2) and possible related omissions of flare peaks,

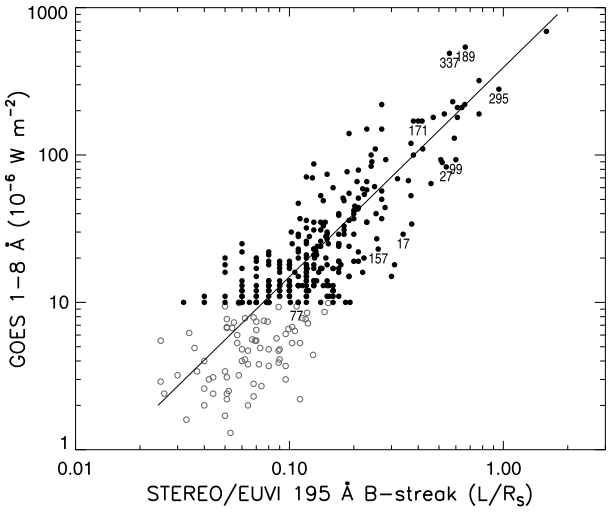

Figure 2 Scatter plot of the relative lengths of the STEREO/EUVI B-streaks versus the GOES 1 – 8 Å fluxes. The gray open circles denote C-class flares, and the black filled circles denote ≥ M1-class flares. The line corresponds to the regression Equation (1). The numbers specify the flares shown in Figures 1, 3, and 4.

– significant differences between impulsive (compact) flares and long-duration events (LDEs, which are usually associated with big CMEs; see below),
– a difference (although small) between the distances of the STEREO-A and B spacecraft from the Sun,
– particularities of the B-streak formation in the blooming process, and
– we measured only the longest B-streak, although several B-streaks occur in some flares (mainly LDEs; see below).

We disregarded these factors for simplicity of the method. Nevertheless, as Figure 2 shows, a clear relationship does indeed exist between the maximum relative length of the B-streak, L/R_S, and the peak GOES 1 – 8 Å flux, F_G. On average, when L/R_S increases from 0.03 to 1.5, F_G rises from 3 to 600 (hereafter F_G is expressed in the unit of 10^{-6} W m^{-2}), which corresponds to the SXR flare class from C3 to X6. The C-class flares confirm the trend of M- and X-class flares. We recall that only a limited number of C flares is presented here and that they were selected randomly and had a conspicuous B-streak. The visibility of short B-streaks is obviously hampered because pre-flare and flaring structures have some longitudinal extent as well. Therefore the points of C-class flares in Figure 2 are biased to relatively longer B-streaks due to their visual selection and the limited number of events. For this reason, we considered only the most powerful flares above the M1.0 level. Because we did not control any of the variables in the $F_G - L/R_S$ relation, the geometric mean regression method was chosen to obtain an empirical dependence between these quantities. Using this method, we obtained a power-law regression equation to fit the relation between the length of the B-streak and the SXR flux,

$$F_G = 392 \times (L/R_S)^{1.42} \quad (1)$$

(the line in Figure 2). The correlation coefficient between L/R_S and F_G is $r \approx 0.81$. For the majority of the $\gtrsim$M1.0 flares, deviations of the SXR flux from the regression line down or up do not exceed a factor of 2. Equation (1) can be used to estimate the SXR fluxes and GOES classes of far-side flares that are observed by STEREO, but are invisible from Earth. We return to this problem in Section 4.

Our analysis shows that many impulsive and LDE flares are characterized by different B-streaks. As Figure 3 demonstrates, in the standard three-day GOES plots, impulsive flares

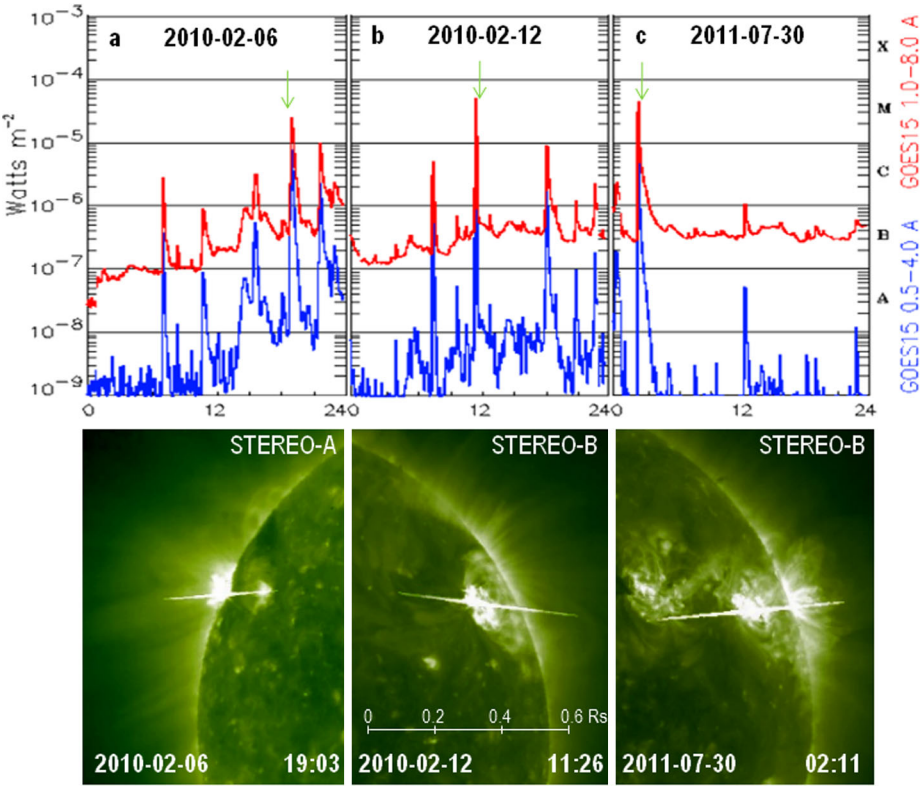

Figure 3 Impulsive GOES M-class flares (upper row) and their thin, single, long B-streaks (bottom). The events on 6 February 2010, 12 February 2010, and 30 July 2011 are labeled 17, 27, and 99 in Figure 2 (see Table 1).

look like spikes almost without any distinct decay phase. In these flares, the whole duration and decay times measured when the flux level decays to a point halfway between the maximum flux and the pre-flare background level, are 10 – 20 minutes and 3 – 10 minutes, respectively. Such a B-streak is usually only visible in two to three EUVI frames of the five-minute cadence. Figure 3 illustrates that impulsive flares produce a single, thin, and relatively long B-streak (see Figure 2 and Table 1). This is because almost the entire flux from these flares is emitted by a single compact core that corresponds to a few pixels. Accordingly, these events reside under the regression line in Figure 2.

In contrast, LDE flares produce relatively short, but thick B-streaks with two or more blooming elements (Figure 4). Apparently, a number of bright source kernels corresponding to these blooming elements contribute to their peak fluxes. In its most developed form, such a multi-element blooming structure does not always temporally coincide with the appearance of the longest B-streak. In the event shown in Figure 4a, several short blooming elements almost merged into one thick B-streak, while in the flares presented in Figures 4b and 4c, the thick part of the B-streak and diffuse core are contained between two thin blooming elements. The LDE flares have noticeably longer durations of 35 – 75 minutes and decay times of 15 – 45 minutes; their multi-element B-streaks are visible in larger numbers of EUVI images (up to 10). We recall that in these events we take into account only the longest B-streak. Feasible summation of the lengths of all visible B-streaks is not always unambiguous and

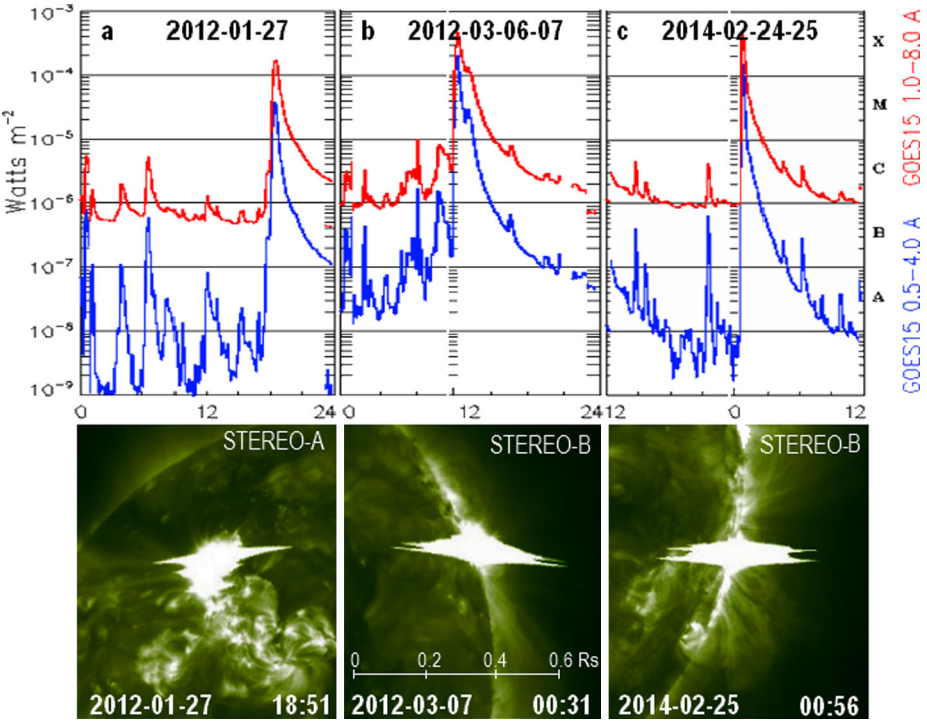

Figure 4 Long-duration GOES X-class flares (upper row) and their thick, two- or multi-element, relatively short B-streaks (bottom). The events on 27 January 2012, 07 March 2012, and 25 February 2014 are labeled 171, 189, and 337 in Figure 2 (see Table 1).

would complicate the method proposed. The fact that we consider only one streak might be the reason why the mentioned LDE events are located above the regression line in Figure 2.

Because the longest B-streaks indicate the brightest flare sources, it is interesting to consider the time difference, Δt, between the observation of such a B-streak in a STEREO/EUVI image, t_S, and a flare peak in the soft X-ray GOES data, t_G. The corresponding histogram for $\geq$M1.0 flares is presented in Figure 5. The time difference does not exceed ± 5 minutes in most events because it is mainly due to the limited imaging rate of EUVI. Practically in all flares with $L/R_S \geq 0.35$, the longest B-streak was observed near the GOES SXR peak. Obviously, $|\Delta t|$ is expected to be small in short-duration flares. Pre-flare heating of brightened erupting filaments or their static extensions produces earlier B-streaks ($\Delta t < 0$).

On the other hand, there is a noticeable percentage of LDEs in which the longest EUV B-streaks were observed with a considerable delay after the SXR peak. Delayed B-streaks with $\Delta t \geq 10$ minutes occurred a few times more often than preceding B-streaks with $\Delta t \leq -5$ minutes. These multiple, relatively short B-streaks in LDEs are produced by many loops of large long-lived arcades. The situation in LDEs is more complex than in impulsive events. Some delayed B-streaks can probably be caused by local brightenings due to the overlap of slowly moving flare loops. Some other delayed B-streaks can be due to subsidiary flare episodes on the background of the long-lasting post-eruption energy release late in such events, almost all of which are associated with large CMEs.

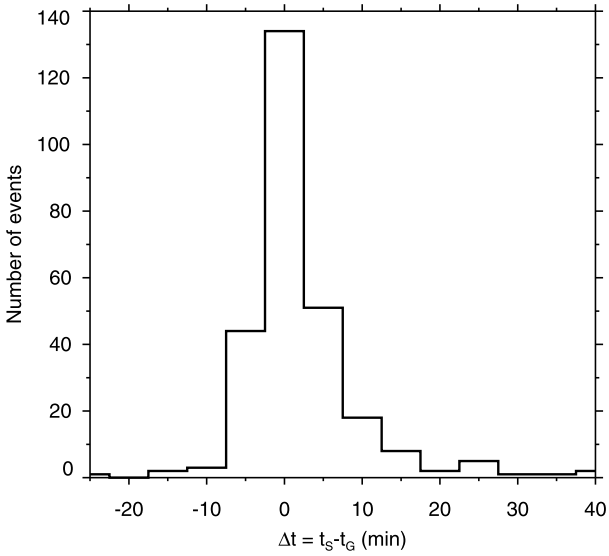

Figure 5 The distribution of the time difference between the observations of the longest STEREO/EUVI B-streak, t_S, and the peak of the SXR flux measured by GOES, t_G, for coincident $\geq$ M1.0 flares.

4. Powerful Far-Side Flares

In this section, we present powerful far-side flares that were not visible from Earth, but were found through B-streaks using a visual inspection of daily STEREO/EUVI movies and images of 2007 – 2014. Almost no such far-side flares were found in 2007 – 2009 for two reasons. Firstly, major flares occurred only rarely during this period of low activity. Secondly, two parts of the solar surface invisible from Earth but observed with STEREO spacecraft were still small. The longitudinal extent of these parts gradually increased, and early in 2011, the whole far-side of the Sun became accessible to STEREO observations. In 2014, both STEREO probes were located almost exactly behind the Sun, and almost all far-side flares were observed by the two spacecraft simultaneously.

The SXR fluxes (GOES classes) of these backside flares were estimated from the relative lengths L/R_S of the longest B-streaks using Equation (1). We restricted ourselves to flares with $L/R_S \geq 0.2$, which corresponds to the GOES class of $\gtrsim$ M4.0. The results are presented in Table 2, where for each of the detected events the following information is listed: the date (1), the time of the longest B-streak (2), the STEREO A or B probe in whose images the streak was measured (3), approximate coordinates of the flare (4), the NOAA number of the active region (5) assigned before its disappearance behind the west limb (mainly for A-probe) or after its appearance at the east limb (mainly for B-probe), the value of the L/R_S parameter (6), the estimated peak SXR flux in units of 10^{-6} W m^{-2} (7), and the flare GOES class (8). In accordance with the small statistical errors of the parameters found in evaluating Equation (1), the 95 % confidence interval of the estimated flare class is rather narrow for short B-streaks and broadens gradually with an increase of L/R_S. For example, the confidence interval is M2.6–M4.7 for an M3.5 flare and X10–X18 for an X13 flare.

Column (9) of Table 2 presents probable ranges of the GOES classes for major far-side flares of 2010 – 2012 estimated by Nitta *et al.* (2013a) from the calculated total DN output. We included all of the 16 backside flares listed by the authors, although three of these flares had $L/R_S < 0.2$. In two of these events (SOL2011-03-21T02:11 and SOL2011-11-03T22:41), the longest B-streaks were even shorter, $L/R_S < 0.1$, but their blooming consisted of many elements, which is typical for LDE flares associated with large CMEs.

Table 2 A list of major far-side flares detected from B-streaks in STEREO/EUVI 195 Å images (see Section 4).

Estimated SXR								
Date	Time UT	A/B	Location	AR	L/R_S	Flux F_G	Class	Nitta *et al.* class range
(1)	(2)	(3)	(4)	(5)	(6)	(7)	(8)	(9)
2010-01-17	03:56	B	S25 E128	11 041	0.54	163	X1.6	M3.4–M9.6
2010-01-19	13:41	B	S25 E95	11 041	0.33	81.2	M8.1	–
2010-01-19	20:36	B	S25 E92	11 041	0.37	95.6	M9.6	–
2010-07-29	08:31	A	N29 W136	–	0.23	48.6	M4.9	–
2010-08-31	20:56	A	S22 W146	11 100	0.49	142.4	X1.4	M8.4–X2.5
2010-09-01	21:51	A	S22 W162	11 100	0.42	114.4	X1.1	M5.4–X1.6
2010-11-03	12:16	B	S19 E98	11 121	0.26*	57.8	M5.8	–
2011-03-21	02:16	A	N17 W129	11 169	0.05*	5.6	C5.6	M1.3–X1.3
2011-06-03	21:06	A	N15 W143	11 222	0.24	51.7	M5.2	–
2011-06-04	07:06	A	N15 W144	11 222	0.32	77.7	M7.8	M5.2–X1.6
2011-06-04	21:51	A	N17 W148	11 222	1.20	508	X5.1	X4.0–X12
2011-08-31	20:06	A	N23 W119	11 278	0.30	70.9	M7.1	–
2011-09-03	02:46	A	N22 W148	11 278	0.31	74.3	M7.4	–
2011-10-18	23:46	A	N15W 130	–	0.33	81.2	M8.1	–
2011-10-19	06:21	A	N14 W134	–	0.27*	61.1	M6.1	–
2011-10-20	03:21	A	N18 W101	11 318	0.20	39.9	M4.0	
2011-10-23	23:16	A	N19 W151	11 318	0.32	77.7	M7.8	M5.3–X1.6
2011-10-26	22:57	B	N18 E167	11 339	0.42	114	X1.1	–
2011-11-03	22:41	B	N09 E154	–	0.09	12.8	M1.3	M4.7–X1.4
2012-03-26	22:56	B	N18 E123	11 451	0.49	142.4	X1.4	M8.2–X2.5
2012-04-26	15:51	A	S23 W123	11 462	0.26	57.8	M5.8	–
2012-04-27	16:06	A	S22 W136	11 462	0.32	77.7	M7.8	–
2012-04-29	12:46	B	N12 E163	11 467	0.77	270	X2.7	M8.3–X2.5
2012-06-12	05:06	A	S15 W126	11 495	0.22	45.7	M4.6	–
2012-07-02	08:36	B	S16 E133	11 520	0.26	57.8	M5.8	–
2012-07-15	15:51	A	S20 W173	11 515	0.22	45.7	M4.6	–
2012-07-23	02:36	A	S15 W133	11 520	0.18	34.3	M3.4	M8.2–X2.5
2012-08-19	18:16	A	S22 W178	11 538	0.24*	51.7	M5.2	–
2012-08-21	20:16	B	S22 E158	11 538	0.28*	64.3	M6.4	M6.8–X2.0
2012-09-11	07:56	B	S22 E178	11 576	0.90	338	X3.4	X1.3–X3.9
2012-09-12	22:56	B	S21 E157	11 576	0.30	70.9	M7.1	–
2012-09-14	20:52	B	N09 E140	11 575	0.27	61.1	M6.1	–
2012-09-15	11:26	B	N09 E131	11 575	0.24	51.7	M5.2	–
2012-09-19	11:16	A	S16 E169	11 582	0.51	151	X1.5	M9.1–X2.7
2012-09-20	15:01	B	S15 E156	11 582	2.38	1343	X13	X5.8–X18
2012-09-22	03:06	B	S16 E135	11 582	0.38	99.2	M9.9	M8.4–X2.5
2012-09-27	10:36	A	S24 W154	11 574	0.30	70.9	M7.1	–
2012-10-08	13:56	B	S29 E107	11 590	0.50	146	X1.5	–
2012-10-19	17:31	A	S21 W156	11 582	0.21	42.7	M4.3	–

Table 2 (*Continued.*)

Estimated SXR								
Date	Time UT	A/B	Location	AR	L/R_S	Flux F_G	Class	Nitta *et al.* class range
(1)	(2)	(3)	(4)	(5)	(6)	(7)	(8)	(9)
2013-04-24	21:46	A	N09 W169	11 719	0.23	48.6	M4.9	–
2013-05-01	02:31	B	N15 E115	11 739	0.32	77.7	M7.8	–
2013-10-05	06:56	B	S23 E125	11 865	0.23	48.6	M4.9	–
2013-10-31	20:25	A	N12 W139	11 880	0.51	151	X1.5	–
2013-11-02	04:26	A	N03 W139	11 875	0.83	301	X3.0	–
2013-11-04	05:21	A	N01 W165	11 875	0.21	42.7	M4.3	–
2013-11-21	00:56	A	S23 W123	11 901	0.42	114	X1.1	–
2013-11-21	16:26	A	S22 W132	11 901	0.25	54.7	M5.5	–
2014-01-06	07:56	A	S15 W113	11 936	0.67	222	X2.2	–
2014-01-26	08:37	B	S16 E107	11 967	0.42	114	X1.1	–
2014-01-31	15:07	B	S14 E155	11 974	0.30	70.9	M7.1	–
2014-02-10	18:16	A	N13 W161	–	0.34*	84.7	M8.5	–
2014-02-11	13:26	A	N09 W112	11 968	0.46	130	X1.3	–
2014-02-14	01:36	A	N08 W137	11 968	0.28	64.3	M6.4	–
2014-02-14	08:26	A	S13 W143	11 967	0.39	103	X1.0	–
2014-02-20	03:16	A	S17 E142	11 990	0.25	54.7	M5.5	–
2014-03-04	18:26	A	N13 W171	–	0.74	256	X2.6	–
2014-03-05	13:26	A	N13 W179	–	1.43	651	X6.5	–
2014-03-06	12:21	A	N12 E166	12 007	0.34*	84.7	M8.5	–
2014-03-09	02:51	A	N17 W159	11 986	0.23	48.6	M4.9	–
2014-05-01	09:31	A	N03 E148	12 056	0.78	275	X2.8	–
2014-05-09	02:31	A	S11 W119	12 051	0.35	88.3	M8.8	–
2014-06-16	02:16	A	S13 W103	12 080	0.20*	39.9	M4.0	–
2014-06-17	09:01	A	S13 W123	12 080	0.28	64.3	M6.4	–
2014-06-30	17:01	B	S21 E125	–	0.26	57.8	M5.8	–
2014-09-01	11:01	B	N14 E129	12 158	0.39	103	X1.0	–
2014-09-01	22:21	B	S14 E121	12 157	0.22	45.7	M4.6	–

Asterisks in column (6) mark the events in which the correction for an exposure time of 8 s was applied.

The third flare of SOL2012-07-23T02:36 with $L/R_S \approx 0.18$ is particularly noteworthy and is discussed below. As Table 2 shows, our analysis of EUVI B-streaks revealed 63 far-side flares above the M4.0 level, including 22 X-class flares, in addition to 94 and 28 flares of the same classes registered by GOES during the ascending and maximum phases of the current solar cycle (until September 2014). Table 2 demonstrates that our estimates of the GOES classes for 13 other major backside flares listed by Nitta *et al.* (2013a) are close to their results as well. In most cases, our estimated GOES importance falls within the range specified by these authors.

Figure 6 illustrates B-streaks in six of the strongest backside flares observed by STEREO/EUVI. Shown in Figure 6c is the SOL2012-09-20 flare with the longest B-streak exceeding the solar diameter; in this case $L/R_S \approx 2.38$, which corresponds to the estimated

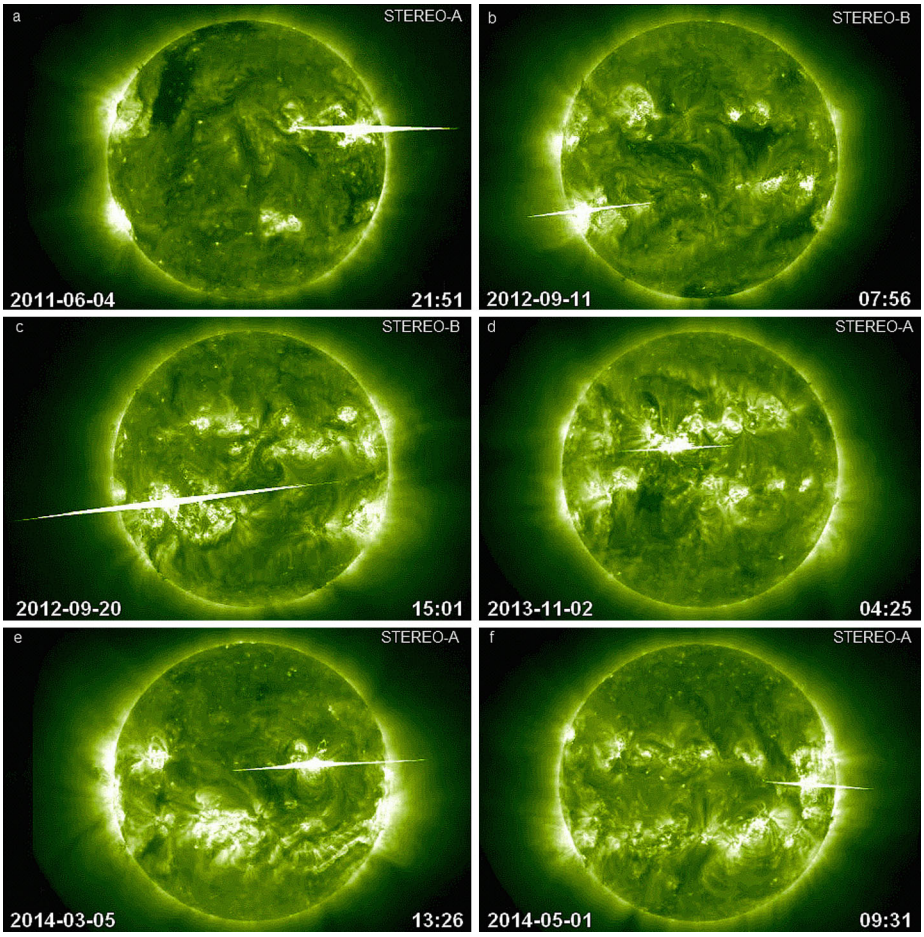

Figure 6 Full-Sun STEREO/EUVI 195 Å images of the six strongest far-side flares detected through B-streaks (see Table 2).

SXR class of X13. This event turned out to be not only the most powerful far-side flare, but the strongest flare of Solar Cycle 24 up to the present time. This conclusion and evaluation of the flare class are consistent with the results of Nitta *et al.* (2013a) obtained through the calculations of the full-disk EUVI total DN output. With an example of this event, we can demonstrate that B-streaks allow not only estimating the SXR importance of large LDE flares, but also reconstructing their probable time history. For this purpose, it is sufficient to have visible B-streaks in several images, to measure their largest relative length, and to calculate the SXR flux using Equation (1). As Figure 7a shows, the B-streaks in the SOL2012-09-20 event are clearly visible, at least, in eight frames of the 5-minute cadence. At the growth phase, a long B-streak appears very sharply. The shape of the time profile indicates that the highest flux occurred between two frames of 14:56 and 15:01. This suggests that the SXR class of this flare was still higher than the longest B-streak implies and seems to be about X20.

Two other far-side events induced interest as sources of outstanding space weather disturbances. The SOL2012-07-23 flare mentioned above is widely debated and considered as

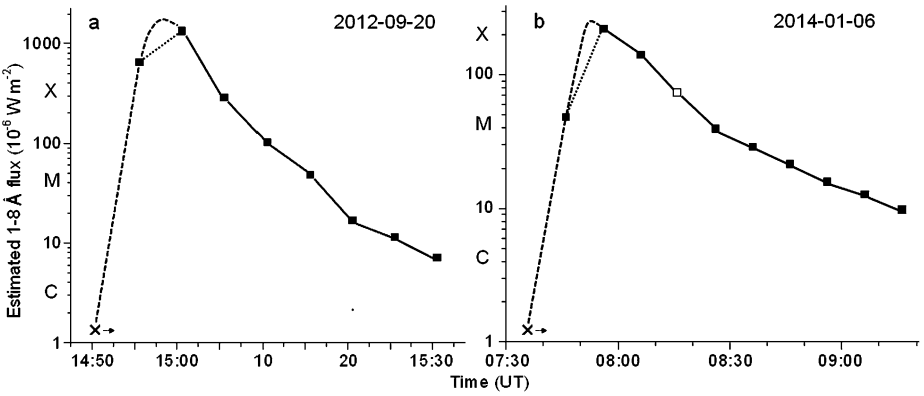

Figure 7 Probable time history of the 1 – 8 Å flux of two famous far-side flares estimated from STEREO/EUVI B-streaks (see the text and Table 2). The crosses with the right arrows correspond to the images in which B-streaks are not yet visible. The dashed lines represent a possible ascending part of the time profiles. The open square in panel (b) refers to an image corrected for an exposure time of 8 s.

an utmost extreme eruptive event (*e.g.*, Ngwira *et al.*, 2013; Liu *et al.*, 2014; Temmer and Nitta, 2015). The corresponding interplanetary CME (ICME) arrived at STEREO-A, which was located favorably, in a very short transit time of 19 – 21 hr and brought to 1 AU a record strong interplanetary magnetic field of 109 nT. If it had been directed toward Earth, this ICME might have caused a geomagnetic storm comparable to the famous Carrington storm of 1859. Meanwhile, the corresponding flare was fairly moderate; Nitta *et al.* (2013a) estimated its soft X-class to be in the M8.2–X2.5 range, and our estimation from the observed B-streak length leads to even lower values of about M5.4. The researchers of this event suggested that the extreme characteristics of the event were caused by a high initial CME speed (up to 3000 km s^{-1}), week ICME drag deceleration in the solar wind determined by preceding solar eruptions and by an enhancement of the magnetic field due to an interaction between two CMEs that closely followed each other. We are currently working on an alternative interpretation suggesting that the extremely high speed of CME/ICME and its strong interplanetary magnetic field were due to a large eruptive magnetic flux and a weak ICME expansion in propagation from the Sun to 1 AU, in accordance with patterns described by Chertok *et al.* (2013) and Grechnev *et al.* (2014). The magnetic flux was estimated from the SDO/HMI magnetogram on 2012-07-12, when the parent active region was located near the center of the visible disk.

The SOL2014-01-06T07:56 flare occurred at a heliolongitude of W113 and produced a 2.5 % ground-level enhancement (GLE) of cosmic rays, only the second one in the unusual Solar Cycle 24. Thakur *et al.* (2014) analyzed this proton event and kinematics of an accompanying CME and concluded that it was consistent with a particle acceleration by a CME-driven shock. On the other hand, a sufficiently long ($L/R_S \approx 0.67$) multi-element B-streak existed in STEREO-A images for nearly one hour during this flare. A probable time history presented in Figure 7b demonstrates that the flare was a powerful LDE of $\approx$X2 class. According to Belov *et al.* (2007), an X2 class flare can well be associated with a source of SEP with proton fluxes of J($>$ 10 MeV) $\approx$120 pfu, J($>$ 100 MeV) $\approx$4.5 pfu, and GLE of $\approx$2 % that are close to the observations. These parameters estimated from B-streaks are typical of flares related to small GLEs.

5. Summary and Concluding Remarks

We have demonstrated how a spurious instrumental effect, which strongly interferes with solar-flare imaging, can provide useful information. Here we studied the so-called blooming, arising from a significant saturation of the STEREO/EUVI 195 Å images in CCD cells corresponding to the cores of sufficiently strong flares. The saturated CCD cells lose their ability to accommodate any additional charge, causing them to spill over into adjacent cells. As a result, one or several bright nearly horizontal streaks (B-streaks) are formed. We showed that in spite of many unaccounted factors, the maximum relative length of the EUV B-streak, L/R_S, correlates with the peak flare SXR flux, F_G, measured by GOES. We analyzed about 350 flares in the period of 2007 – 2014 that were observed simultaneously by GOES and at least one of STEREO spacecraft, and established an empirical relation between L/R_S and F_G. This allowed us to propose a simple and prompt method for estimating the SXR class of far-side flares that are observed with STEREO, but are invisible for GOES.

The method consists of a direct measurement of the length of the longest B-streak in units of the solar radius in the routine EUVI 195 Å images or movies, accessible in near real time at http://stereo-ssc.nascom.nasa.gov/browse/, and the use of Equation (1). It is only necessary to ensure that all the measurements were converted to the exposure time of 8 s. Before this, Nitta *et al.* (2013a) proposed a somewhat more laborious method for estimating the SXR flux and class of far-side flares based on calculations of the EUVI full-disk total digital number output. It should be noted that if there is a temporal overlap between the flares in different active regions, then our method enables measuring their B-streaks and estimating their classes independently of each other.

Applying our method to the STEREO observations during the ascending and maximum phases of Solar Cycle 24 allowed us to find about 65 major far-side flares with the EUVI B-streak lengths of $L/R_S \geq 0.2$ and to estimate their SXR fluxes and classes. For most of the 16 far-side flares listed by Nitta *et al.* (2013a) for 2010 – 2012, our estimates are close to their results. Of these events, the SOL2012-09-20 flare is the strongest one in the current solar cycle. Its probable importance of about X13 was estimated from $L/R_S \approx 2.38$. We also briefly discussed two far-side events of interest for space weather. The SOL2012-07-23 eruption occurred in an active region with a strong magnetic flux that for a favorable location relative to Earth could have been the source of an extremely strong and prompt geomagnetic storm. Judging from the B-streak, the west behind-the-limb flare of 2014-01-06 was sufficiently intense and long-lasting to be connected with the source of the observed proton event including a GLE.

Using the two LDE events as examples, we demonstrated that by measuring the maximum B-streak length in a number of consecutive images, one can reconstruct the probable time history of a flare. It is clear that these and other features found due to B-streaks require a more detailed study. Hopefully, the proposed simple method of prompt estimations of the SXR class of the far-side STEREO flares from spurious B-streaks is useful for solar studies and solar-terrestrial forecasting.

Acknowledgements We are grateful to the anonymous referee for constructive comments that helped us to improve the manuscript. The authors thank the GOES and STEREO teams for their open data used in our study. This research was supported by the Russian Foundation of Basic Research under grant 14-02-00367 and the Ministry of Education and Science of Russian Federation under projects 8407 and 14.518.11.7047.

References

Andrews, M.D.: 2001, *Solar Phys.* **204**, 181. DOI.

Aschwanden, M.J., Wülser, J.-P., Nitta, N.V., Lemen, J.R., Freeland, S., Thompson, W.T.: 2014, *Solar Phys.* **289**, 919. DOI.

Belov, A., Kurt, V., Mavromichalaki, H., Gerontidou, M.: 2007, *Solar Phys.* **246**, 457. DOI.
Chertok, I.M., Grechnev, V.V., Belov, A.V., Abunin, A.A.: 2013, *Solar Phys.* **282**, 175. DOI.
Delaboudinière, J.-P., Artzner, G.E., Brunaud, J., Gabriel, A.H., Hochedez, J.F., Millier, F., Song, X.Y., Au, B., Dere, K.P., Howard, R.A., *et al.*: 1995, *Solar Phys.* **162**, 291. DOI.
Garcia, H.A.: 1994, *Solar Phys.* **154**, 275. DOI.
Grechnev, V.V., Uralov, A.M., Chertok, I.M., Belov, A.V., Filippov, B.P., Slemzin, V.A., Jackson, B.V.: 2014, *Solar Phys.* **289**, 4653. DOI.
Howard, R.A., Moses, J.D., Vourlidas, A., Newmark, J.S., Socker, D.G., Plunkett, S.P.: 2008, *Space Sci. Rev.* **136**, 67. DOI.
Hudson, H.S.: 2011, *Space Sci. Rev.* **158**, 5. DOI.
Kaiser, M.L., Kucera, T.A., Davila, J.M., St. Cyr, O.C., Guhathakurta, M., Christian, E.: 2008, *Space Sci. Rev.* **136**, 5. DOI.
Kwon, R.-Y., Zhang, J., Vourlidas, A.: 2015, *Astrophys. J. Lett.* **799**, L29. DOI.
Lemen, J.R., Title, A.M., Akin, D.J., Boerner, P.F., Chou, C., Drake, J.F., Duncan, D.W., Edwards, C.G., Friedlaender, F.M., Heyman, G.F., *et al.*: 2012, *Solar Phys.* **275**, 17. DOI.
Li, Y., Luhmann, J.G., Lynch, B.J., Kilpua, E.K.J.: 2014, *J. Geophys. Res.* **119**, 3237. DOI.
Liu, Y.D., Luhmann, J.G., Kajdič, P., Kilpua, E.K.J., Lugaz, N., Nitta, N.V., Möstl, C., Lavraud, B., Bale, S.D., Farrugia, C.J., Galvin, A.B.: 2014, *Nat. Commun.* **5**, 3481. DOI.
Lugaz, N., Kintner, P., Möst, C., Jian, L.K., Davis, C.J., Farrugia, C.J.: 2012, *Solar Phys.* **279**, 497. DOI.
Ngwira, C.M., Pulkkinen, A., Leila Mays, M., Kuznetsova, M.M., Galvin, A.B., Simunac, K., Baker, D.N., Li, X., Zheng, Y., Glocer, A.: 2013, *Space Weather* **11**, 671. DOI.
Nitta, N.V., Aschwanden, M.J., Boerner, P.F., Freeland, S.L., Lemen, J.R., Wuelser, J.-P.: 2013a, *Solar Phys.* **288**, 241. DOI.
Nitta, N.V., Schrijver, C.J., Title, A.M., Liu, W.: 2013b, *Astrophys. J.* **776**, 58. DOI.
Richardson, I.G., von Rosenvinge, T.T., Cane, H.V., Christian, E.R., Cohen, C.M.S., Labrador, A.W., Leske, R.A., Mewaldt, R.A., Wiedenbeck, M.E., Stone, E.C.: 2014, *Solar Phys.* **289**, 3059. DOI.
Schwartz, R.A., Torre, G., Piana, M.: 2014, *Astrophys. J. Lett.* **793**, L23. DOI.
Temmer, M., Nitta, N.: 2015, *Solar Phys.* **290**, 919. DOI.
Thakur, N., Gopalswamy, N., Xie, H., Mäkelä, P., Yashiro, S., Akiyama, S., Davila, J.M.: 2014, *Astrophys. J. Lett.* **790**, L13. DOI.
Webb, D.F., Howard, T.A.: 2012, *Living Rev. Solar Phys.* **9**, 3. DOI.
Wuelser, J.-P., Lemen, J.R., Tarbell, T.D., Wolfson, C.J., Cannon, J.C., Carpenter, B.A., Duncan, D.W., Gradwohl, G.S., Meyer, S.B., Moore, A.S., *et al.*: 2004, In: Fineschi, S., Gummin, M.A. (eds.) *Telescopes and Instrumentation for Solar Astrophysics*, *Proc. SPIE* **5171**, 111. DOI.